Carrier mobility tensor in doped phosphorene due to scattering by charged impurities using the energy loss method

Milad Moshayedi and Z. L. Mišković *
Department of Applied Mathematics, University of Waterloo, Waterloo, Ontario, Canada N2L 3G1

(Received 16 October 2023; revised 16 November 2023; accepted 22 November 2023; published 6 December 2023)

We use the energy loss method (ELM) to evaluate the drift mobility tensor of doped phosphorene due to scattering of its carriers on an ensemble of charged impurities located in a substrate. The ELM makes it possible to circumvent the endeavor of numerically solving the Boltzmann transport equation for the same problem, whereby it yields an explicit expression for the mobility tensor components as a double integral, making it straightforward to survey various model layouts and parameters. This enabled us to perform a statistical analysis of the effects of spatial correlation among the impurities by means of a geometric structure factor for the hard-disk model of a planar distribution of pointlike impurities. We found that the correlation distance between impurities plays an important role at doping densities of phosphorene that are lower than the areal density of impurities. Moreover, the ELM naturally brings about the dielectric function of phosphorene, allowing us to explore the role of interband electron transitions in static screening of the impurities, in addition to the role played by the intraband transitions, which we treat in the random phase approximation. We found that the interband transitions augment the screening when impurities are close to phosphorene and when its doping density increases, thereby increasing the mobility tensor components while decreasing their asymmetry ratio.

DOI: 10.1103/PhysRevB.108.245404

I. INTRODUCTION

Phosphorene is a single layer of black phosphorus, which has attracted a great deal of interest over the past decade [1–3] as a monoelemental two-dimensional (2D) semiconductor, whose puckered atomic lattice structure gives rise to strong anisotropy of its mechanical, electronic, optical, and transport properties with a plethora of possible applications [4–7]. In the area of nanoelectronic devices [8], measurements of transport properties of phosphorene are still scarce [2,9,10], while the agreement of experiments with theory remains insufficient, at least when modeling of the carrier-phonon scattering mechanism at room temperature is concerned [11]. On the other hand, modeling of the drift mobility tensor for an anisotropic 2D material due to its carrier scattering on charged impurities (CIs) at low temperature by means of the linearized Boltzmann transport equation (BTE) is greatly complicated by the need to solve numerically an integral equation for momentum relaxation time (MRT) that depends on the direction of the applied electric field [12–16]. This points to a serious limitation of the BTE when it comes to exploring various designs of nanoelectronic devices based on phosphorene [8,10,11], and, more importantly, it makes it extremely computationally costly, if not impossible, to use the BTE to study the effects of a spatial arrangement of CIs on the mobility of phosphorene.

An elegant but far less favored approach than the BTE to calculating the drift mobility is based on the energy loss method (ELM). [17–19] The idea behind the ELM in the case of carrier scattering on CIs is simple: it rests on the Galilean transformation between the laboratory frame where the impurities are at rest and the frame moving with constant drift velocity of charge carriers in the conducting material [20–24], coupled with an equivalence of the energy loss rate for the moving impurities and the Joule heat released in the material [25]. The ELM has several advantages over the BTE approach. First, it eliminates the need to introduce MRT, but rather uses the dielectric function for intraband electronic transitions in a 2D conducting material, which only needs to be available to the leading order in frequency [17,18]. Using dielectric functions at various degrees of approximation enables straightforward inclusion of various material properties into the mobility calculations, such as the anisotropy of the band structure [12,14–16], finite temperature [13], or contribution of interband transitions to the static screening of the impurity potential [26–30]. Second, the ELM completely avoids the need to solve an integral equation for MRT of the BTE approach, but rather yields an explicit expression for the drift mobility, or the dc electric conductivity of the material in terms of an integral, which includes a properly screened external potential on which the charge carriers are scattered. This makes it straightforward to explore variations in the arrangement of the nearby dielectrics via the Green's function (GF) of the Poisson equation [31], as well as to study various external scattering centers for charge carriers, which are not necessarily limited to CIs. For example, the ELM was used to describe electron scattering on interface roughness [32], polarizable scattering centers [33], and dislocations in semiconductors [24]. The ELM was also used for mobility calculations in a quasi-2D electron gas [34] and graphene

*Also at Waterloo Institute for Nanotechnology, University of Waterloo, Waterloo, Ontario, Canada; zmiskovi@uwaterloo.ca

[31], with the latter work exploring the effects of spatial correlation among the CIs by means of a geometric structure factor.

While all the above implementations of the ELM were concerned with isotropic conducting materials, in this work we adapt the ELM to the case of an anisotropic 2D material by choosing a dielectric function that describes single band occupancy of an electron doped phosphorene [12,14,16], and we apply it to the carrier scattering on an arbitrary distribution of pointlike CIs in an SiO_2 substrate, as in Ref. [31]. We derive expressions for the mobility tensor in the zero-temperature limit, corresponding to the case studied in Ref. [12], but note that generalizations can be readily made to the regime of finite temperature [13] and to phosphorene encapsulated between two dielectrics [8,10] by using the GFs from Ref. [31]. We first show that our expressions for the mobility tensor components reproduce the results of a numerical solution of the BTE presented in Ref. [12] when we use their model parameters. We then continue by using the phosphorene parameters deduced from *ab initio* calculations by Novko *et al.* [29], and we explore the effects of the interband electron transitions in static screening of the impurity potential [30], the finite gap between phosphorene and the substrate [31], and the effects of finite correlation distance between impurities using the hard-disk (HD) model parametrized by Rosenfeld [35]. While we do not aim to reproduce experimental data on the mobility of phosphorene, we advocate in this work in favor of the ELM as a powerful alternative to the BTE in the case of phosphorene and other anisotropic materials, which can readily tackle a significantly expanded set of model systems of interest for designing future nanoelectronic devices [8,10].

II. THEORETICAL MODEL

Using a Cartesian coordinate system with the coordinates $\mathbf{R} \equiv \{\mathbf{r}, z\}$, where $\mathbf{r} = \{x, y\}$, we assume that a flat phosphorene sheet of large area A is placed in vacuum at the height $h \geqslant 0$ above the planar surface of a substrate with (relative) dielectric constant ϵ_s, which occupies the half-space $z \leqslant 0$ and contains a large number N of pointlike impurities, each carrying a charge of Ze ($e > 0$ being the proton charge). We assume that the impurities are statistically distributed, having the charge density described by $\rho_0(\mathbf{r}, z)$ in the laboratory frame, which is translationally invariant in the directions of $\mathbf{r}$. An ensemble average over the geometric arrangements of the impurities, denoted by $\langle \cdots \rangle$, gives an average density $\langle \rho_0(\mathbf{r}, z) \rangle \equiv \bar{\rho}_0(z)$ that may only depend on the perpendicular distance z. This average does not participate in the carrier scattering in phosphorene, but its integral, $\int dz\, \bar{\rho}_0(z) = Ze\, n_{\rm imp}$ with $n_{\rm imp} = \frac{N}{A}$ being the areal density of impurities, defines (in conjunction with the applied gate voltage) the doping of phosphorene with electrons or holes having an equilibrium areal density n. On the other hand, the carrier scattering is governed by the fluctuation part of the CI density, $\delta\rho_0(\mathbf{r}, z) = \rho_0(\mathbf{r}, z) - \bar{\rho}_0(z)$.

A. Energy loss method

The ELM is based on a thought experiment pertaining to a conductivity measurement [18,21,24], which assumes that a (weak but otherwise arbitrary) constant electric field $\mathbf{E}$ is applied tangentially to phosphorene where it induces an in-plane drift current $\mathbf{J}_d$, so that the total Joule power released in phosphorene is $P_{\rm J} = \iint d^2\mathbf{r}\, \mathbf{J}_d \cdot \mathbf{E} = A\mathbf{J}_d \cdot \mathbf{E}$. Expressing the current in terms of a (constant) drift velocity $\mathbf{v}_d$ of charge carriers in an (electron-doped) phosphorene as $\mathbf{J}_d = -en\mathbf{v}_d$, one may invoke Ohm's law in the form $\mathbf{J}_d = \overleftrightarrow{\sigma} \cdot \mathbf{E}$, where $\overleftrightarrow{\sigma}$ is the in-plane dc conductivity tensor of phosphorene, which can be expressed in terms of the mobility tensor as $\overleftrightarrow{\sigma} = -en\overleftrightarrow{\mu}$. Therefore, we have $P_{\rm J} = -Aen\mathbf{v}_d \cdot \mathbf{E}$ and the relation $\mathbf{v}_d = \overleftrightarrow{\mu} \cdot \mathbf{E}$, which may be used to eliminate the electric field in terms of the (small but otherwise arbitrary) drift velocity to finally express the Joule power as

$$P_{\rm J} = -Aen\, \mathbf{v}_d \cdot \overleftrightarrow{\mu}^{-1} \cdot \mathbf{v}_d, \tag{1}$$

where $\overleftrightarrow{\mu}^{-1}$ is the inverse of the mobility tensor of phosphorene.

The equivalence principle invoked in the ELM by reversing the frames of reference asserts that the Joule power in the conductivity experiment with drifting carriers in phosphorene is equal to the energy lost by the system of CIs that moves rigidly with the opposite velocity $\mathbf{v} = -\mathbf{v}_d$ parallel to a frame where phosphorene with zero drift is at rest. In that frame, the fluctuation part of the CI density, given by $\delta\rho(\mathbf{R}, t) = \delta\rho_0(\mathbf{r} - \mathbf{v}t, z)$, induces an electrostatic potential, $\delta\Phi_{\rm pol}(\mathbf{R}, t)$, due to polarization of charge carriers in phosphorene away from their equilibrium state with zero drift. This potential may be expressed via the GF of the Poisson equation, which takes into account static screening by the nearby dielectrics as [31]

$$\delta\Phi_{\rm pol}(\mathbf{R}, t) = \iiint d^3\mathbf{R}' \int dt'\, G_{\rm pol}(\mathbf{R}, \mathbf{R}'; t - t')\, \delta\rho(\mathbf{R}', t'). \tag{2}$$

Assuming translational invariance of the structure, we may perform the Fourier transform (FT) with respect to the in-plane coordinates ($\mathbf{r} \to \mathbf{q} = \{q_x, q_y\}$) and time ($t \to \omega$), allowing us to rewrite the above relation (using the tilde to denote the transformed functions) as

$$\delta\widetilde{\Phi}_{\rm pol}(\mathbf{q}, z, \omega) = \int_{-\infty}^{\infty} dz'\, \widetilde{G}_{\rm pol}(\mathbf{q}; z, z'; \omega)\, \delta\widetilde{\rho}(\mathbf{q}, z', \omega), \tag{3}$$

where

$$\begin{aligned}\delta\widetilde{\rho}(\mathbf{q}, z, \omega) &= \iint d^2\mathbf{r} \int_{-\infty}^{\infty} dt\, e^{-i\mathbf{q}\cdot\mathbf{r} + i\omega t}\, \delta\rho_0(\mathbf{r} - \mathbf{v}t, z) \\ &= 2\pi\, \delta(\omega - \mathbf{q}\cdot\mathbf{v})\, \delta\widetilde{\rho}_0(\mathbf{q}, z)\end{aligned} \tag{4}$$

with the δ function in the second line expressing the Galilean transformation between the moving frame and the rest frame of phosphorene. Here, $\delta\widetilde{\rho}_0(\mathbf{q}, z) = \widetilde{\rho}_0(\mathbf{q}, z) - (2\pi)^2\, \delta(\mathbf{q})\, \bar{\rho}_0(z)$ is the FT of the fluctuating part of the CI density with respect to the in-plane coordinates in the laboratory frame, where impurities are at rest.

The energy loss rate of the moving system of CIs can be obtained from

$$P_{\rm imp} = \iiint d^3\mathbf{R}\, \mathbf{J}_{\rm imp}(\mathbf{R}, t) \cdot \mathbf{E}_{\rm pol}(\mathbf{R}, t), \tag{5}$$

where $\mathbf{J}_{\rm imp}(\mathbf{R}, t) = \mathbf{v}\delta\rho_0(\mathbf{r} - \mathbf{v}t, z)$ is the associated current density, and $\mathbf{E}_{\rm pol}(\mathbf{R}, t) = -\nabla_{\mathbf{r}}\delta\Phi_{\rm pol}(\mathbf{r}, z, t)$ is the polarization

electric field parallel to phosphorene. Switching to the FT and using Eqs. (3) and (4) in Eq. (5) allows us to write an ensemble average of the impurity energy loss rate as

$$\langle P_{\rm imp}\rangle = -i\iint \frac{d^2\mathbf{q}}{(2\pi)^2}\,(\mathbf{q}\cdot\mathbf{v})\int dz\int dz'\,\widetilde{G}_{\rm pol}(\mathbf{q};z,z';\mathbf{q}\cdot\mathbf{v}) \times \langle\delta\widetilde{\rho}_0(-\mathbf{q},z)\delta\widetilde{\rho}_0(\mathbf{q},z')\rangle. \tag{6}$$

Taking into account the relevant symmetries in the FT domain (see Appendix A), the above expression may be cast for the configuration of dielectrics used in this work in the following form:

$$\langle P_{\rm imp}\rangle = -NZ^2\iint \frac{d^2\mathbf{q}}{(2\pi)^2}\,(\mathbf{q}\cdot\mathbf{v})\,V_{\rm C}(q)\left[\frac{\epsilon_{\rm bg}(q)}{\epsilon^0_{\rm bg}}\right]^2 e^{-2qh} \times \mathcal{S}(\mathbf{q})\,{\rm Im}\left[\frac{-1}{\epsilon(\mathbf{q},\mathbf{q}\cdot\mathbf{v})}\right], \tag{7}$$

where $V_{\rm C}(q) = 2\pi e^2/q$ is the in-plane FT of the Coulomb potential with $q = \sqrt{q_x^2+q_y^2}$, and

$$\epsilon_{\rm bg}(q) = \left[1-\frac{\epsilon_s-1}{\epsilon_s+1}\exp(-2qh)\right]^{-1} \tag{8}$$

is a background dielectric function describing static screening due to dielectric(s) surrounding phosphorene, which takes the well-known form $\epsilon^0_{\rm bg} = (\epsilon_s+1)/2$ in the limit of zero gap, $h = 0$ [12,14]. The loss function ${\rm Im}[-1/\epsilon(\mathbf{q},\omega)]$ appearing in Eq. (7), which describes energy dissipation due to the polarization of phosphorene, is expressed in terms of an effective 2D dielectric function of phosphorene defined as

$$\epsilon(\mathbf{q},\omega) = \epsilon_{\rm bg}(q) + V_{\rm C}(q)\,\chi(\mathbf{q},\omega), \tag{9}$$

where $\chi(\mathbf{q},\omega)$ is the density-density dynamic response function of phosphorene. A statistical description of the geometric structure of the CIs is included in Eq. (7) via the structure factor $\mathcal{S}(\mathbf{q})$, which is discussed next.

B. Structure factor of charged impurities

We define an effective 2D structure factor of the CIs residing in the substrate at $z \leqslant 0$ as [31]

$$\mathcal{S}(\mathbf{q}) = \frac{1}{Ne^2Z^2}\int_{-\infty}^{0} dz\int_{-\infty}^{0} dz'\,e^{q(z+z')}\langle\delta\widetilde{\rho}_0(-\mathbf{q},z)\delta\widetilde{\rho}_0(\mathbf{q},z')\rangle. \tag{10}$$

Assuming that the impurities occupy sites $\mathbf{R}_j \equiv \{\mathbf{r}_j, z_j\}$ in the laboratory frame with $z_j \leqslant 0$ for $j = 1, 2, \ldots, N$, their charge density is given by

$$\rho_0(\mathbf{r},z) = eZ\sum_{j=1}^{N}\delta(\mathbf{r}-\mathbf{r}_j)\,\delta(z-z_j). \tag{11}$$

Statistical properties of the distribution of the impurity positions may be modeled by assuming translational invariance of their structure in the $\mathbf{r}$ directions and using the one- and two-particle distribution functions [36],

$$F_1(\mathbf{r},z) = \frac{N}{A}f_1(z) \tag{12}$$

and

$$F_2(\mathbf{r}_1,\mathbf{r}_2;z_1,z_2) = \frac{N(N-1)}{A^2}f_1(z_1)f_1(z_2) \times g(\mathbf{r}_2-\mathbf{r}_1;z_1,z_2). \tag{13}$$

Here, $f_1(z)$ describes the distribution of particle positions in the perpendicular direction, which is nonzero for $z \leqslant 0$ and is normalized to 1, whereas $g(\mathbf{r};z_1,z_2)$ is related to the usual *radial distribution* function having the limit $g \to 1$ as $r \equiv \|\mathbf{r}\| \to \infty$ [36]. With these specifications and additionally assuming that the impurities are isotropically distributed in the directions parallel to phosphorene, the structure factor is finally obtained as (see Appendix B)

$$\mathcal{S}(q) = \int_{-\infty}^{0} dz\,f_1(z)\,{\rm e}^{2qz} + 2\pi n_{\rm imp}\int_{-\infty}^{0} dz_1\,f_1(z_1)\,{\rm e}^{qz_1} \times \int_{-\infty}^{0} dz_2\,f_1(z_2)\,{\rm e}^{qz_2}\int_0^{\infty} dr\,rJ_0(qr) \times [g(r;z_1,z_2)-1], \tag{14}$$

where J_0 is a Bessel function of zeroth order.

It is difficult to model a full three-dimensional (3D) structure of CIs in the substrate in the presence of correlation, which is largely unknown anyway (see Appendix B of Ref. [31]), so we shall only consider two special cases. An ensemble of spatially uncorrelated impurities is defined by setting $g = 1$ in Eq. (14), leaving only the first term to describe the impurity distribution along the z axis [14,31]. In this case, we shall consider a uniform 3D distribution over the layer of finite thickness L in the substrate, as in Ref. [12], defined by $f_1(z) = 1/L$ for $-L \leqslant z \leqslant 0$, which gives $\mathcal{S}(q) = (1-e^{-2qL})/(2qL)$ from Eq. (14). A more frequently used model in the literature assumes a planar distribution of impurities at constant depth $d \geqslant 0$ from the surface of the substrate with no spatial correlation among the impurities, which is recovered by setting $f_1(z) = \delta(z+d)$ and $g = 1$ in Eq. (14), thereby giving $\mathcal{S}(q) = {\rm e}^{-2qd}$ [12,14,31].

However, we shall explore the role of correlation among the impurities within a planar distribution by setting $f_1(z) = \delta(z+d)$ and invoking the HD model in Eq. (14), which yields $\mathcal{S}(q) = {\rm e}^{-2qd}S_{\rm HD}(q)$, where for the HD structure factor $S_{\rm HD}(q)$ we use Resenfeld's parametrization [35], as given in Eq. (B1) of Ref. [31]. A key parameter of the HD model is packing fraction $p = \pi n_{\rm imp}r_c^2/4$, where r_c is the correlation distance between the impurities, which will be seen to give rise to a deviation from the simple inverse proportionality of the mobility with the average impurity density $n_{\rm imp}$ for increasing r_c values. We note that Resenfeld's parametrization of $S_{\rm HD}(q)$ provides reasonably accurate representation of the HD model up to quite large packing fractions of $p \approx 0.69$ [35].

For small packing fractions, the HD structure factor exhibits week oscillations about the value $S_{\rm HD}(q) = 1$ characterizing uncorrelated impurities ($r_c = 0$), with the peaks located close to the values $q_\ell = 2\pi\ell/r_c$, where $\ell = 1, 2, \ldots$, which correspond to the ℓth coordination shell of the HD model [35,36]. As p increases, $S_{\rm HD}(q)$ is dominated by a strong peak at q_1 corresponding to the first coordination shell, followed by heavily damped oscillations peaking at

subsequent coordination shells, and ultimately reaching the value of $S_{\rm HD}(q) = 1$ as $q \to \infty$. On the other hand, at long wavelengths, $q < q_1$, the magnitude of the HD structure factor is strongly reduced for increased packing fraction, reaching the value of $S_{\rm HD}(0) = (1-p)^3/(1+p)$ as $q \to 0$ [31].

C. Polarization function of doped phosphorene

The density-density polarization function of doped phosphorene in the random phase approximation includes contributions from both the intraband and interband electron transitions, $\chi(\mathbf{q},\omega) = \chi_{\rm intra}(\mathbf{q}) + \chi_{\rm inter}(\mathbf{q},\omega)$ [29]. Without loss of generality, we shall consider n-doped phosphorene with an electron density n and assume that the Fermi level only crosses the lowest conduction band (see Fig. 5 in Ref. [29]). It was shown that, for the purpose of the mobility calculations [14], the electron energy dispersion may be approximated near the Γ point of the Brillouin zone by $\varepsilon_{\mathbf{k}} = \frac{\hbar^2 k_x^2}{2m_x} + \frac{\hbar^2 k_y^2}{2m_y}$ with respect to the band bottom. Here, m_x and m_y are the effective electron masses in the directions along the principal axes of the phosphorene lattice, labeled the armchair (AC) and zigzag (ZZ) directions, respectively [12,14,16]. With this energy band approximation for charge carriers in phosphorene, the intraband polarization function may be obtained as [16,28]

$$\chi_{\rm intra}(\mathbf{q},\omega) = \chi_{\rm iso}(Q,\omega), \tag{15}$$

where $\chi_{\rm iso}(Q,\omega)$ is the polarization function of an equivalent *isotropic* 2D electron gas (2DEG), which has the same doping density, n, and the electron mass defined by $m_d = \sqrt{m_x m_y}$, whereas its wave number Q is a function of the wave vector $\mathbf{q} = \{q_x, q_y\}$ and the effective electron masses of phosphorene, given by

$$Q(\mathbf{q}) = \sqrt{q_x^2\sqrt{\frac{m_y}{m_x}} + q_y^2\sqrt{\frac{m_x}{m_y}}}. \tag{16}$$

For our purpose, it suffices to use Lindhard's function of an isotropic 2DEG [37,38] as a model for $\chi_{\rm iso}(Q,\omega)$. Namely, we only need an approximation for Eq. (7) to the second order in the velocity $\mathbf{v}$ so that it may be compared with Eq. (1). This requires a linear approximation for the frequency dependence of the loss function $\mathrm{Im}[-1/\epsilon(\mathbf{q},\omega)]$ [17,18], which may be deduced from the linearization of the Lindhard function for a degenerate 2DEG at zero temperature [39,40],

$$\chi_{\rm iso}(Q,\omega) \approx \frac{m_d}{\pi\hbar^2}\left[1 - \frac{1}{Q}\sqrt{Q^2 - (2k_{\rm F})^2}H(Q-2k_{\rm F})\right] + i\omega\frac{2m_d^2}{\pi\hbar^3 Q}\frac{H(2k_{\rm F}-Q)}{\sqrt{(2k_{\rm F})^2 - Q^2}}, \tag{17}$$

where $H(\cdot)$ is the Heaviside function, and $k_{\rm F} = \sqrt{2\pi n}$ is the Fermi wave number. To include the effect of finite temperature [13], one should apply Maldague's formula to the above expression [41], but this goes beyond our goal in this work.

As for the interband contribution to the polarization function of phosphorene, it was shown that for frequencies $\hbar\omega \lesssim E_g/2$, where $E_g \approx 2$ eV is its gap energy, and for the wave numbers $q \lesssim 1$ nm^{-1}, it is an excellent approximation to use the static limit [28,42] along with the long-wavelength limit [29,30], which give

$$\chi_{\rm inter}(\mathbf{q}) = \frac{1}{e^2}\left(\alpha_x q_x^2 + \alpha_y q_y^2\right), \tag{18}$$

where α_x and α_y are the static in-plane polarizabilities due to the interband transitions in the AC and the ZZ directions, respectively [29,43]. Thus, combining Eq. (18) with Eq. (15) where we employ the approximation in Eq. (17) gives the effective dielectric function of phosphorene in Eq. (9), which can be used to obtain the loss function to the linear order in frequency. Upon substitution $\omega = \mathbf{q}\cdot\mathbf{v}$, this gives an expression for the loss function to be used in Eq. (7) as

$$\mathrm{Im}\left[\frac{-1}{\epsilon(\mathbf{q},\mathbf{q}\cdot\mathbf{v})}\right] = \frac{\mathbf{q}\cdot\mathbf{v}}{[\epsilon_{\rm stat}(\mathbf{q})]^2}\frac{k_{\rm TF}}{q}\frac{2m_d}{\hbar Q}\frac{H(2k_{\rm F}-Q)}{\sqrt{(2k_{\rm F})^2 - Q^2}}, \tag{19}$$

where $k_{\rm TF} = 2m_d e^2/\hbar^2$ is the Thomas-Fermi inverse screening length of the equivalent isotropic 2DEG, and $\epsilon_{\rm stat}(\mathbf{q})$ is a static dielectric function of phosphorene, defined in the presence of the interband contribution as [29]

$$\epsilon_{\rm stat}(\mathbf{q}) = \epsilon_{\rm bg}(q) + \frac{2\pi}{q}\left(\alpha_x q_x^2 + \alpha_y q_y^2\right) + \frac{k_{\rm TF}}{q} \tag{20}$$

for wave vectors constrained by the condition $Q(\mathbf{q}) < 2k_{\rm F}$, which follows from Eq. (19) with $Q(\mathbf{q})$ given in Eq. (16).

Several comments are in order regarding the function in Eq. (20). It generalizes the Rytova-Keldysh model dielectric function, which is often used for static screening of the Coulomb interaction in modeling excitons in 2D semiconductors [26,27,29]. In the dynamic regime, when the intraband transitions may be approximated by a Drude form of the intraband contribution $\chi_{\rm intra}(\mathbf{q},\omega)$, the presence of the terms with static polarizabilities $\alpha_{x/y}$ in Eq. (20) gives rise to a saturation of the sheet plasmon dispersion with increasing wave numbers, accompanied by "slowing down" of that plasmon [42,44,45]. On the other hand, even though any asymmetry between static polarizabilities α_x and α_y implies anisotropic static screening by the function $\epsilon_{\rm stat}(\mathbf{q})$ in Eq. (20), the primary effects of anisotropy in the mobility will be seen to arise from the asymmetry between the effective masses in the function Q, Eq. (16). This becomes especially clear at low doping densities of phosphorene, where a regime of the so-called "complete screening" is achieved for $n \to 0$ (see below) [16], when the dielectric function in Eq. (20) is dominated by the Thomas-Fermi term, $k_{\rm TF}/q$.

D. Expression for the mobility tensor of phosphorene

When Eq. (19) is substituted into Eq. (7) for $\langle P_{\rm imp}\rangle$, the integrand will contain a factor $(\mathbf{q}\cdot\mathbf{v})^2$, which may be written as $\mathbf{v}\cdot(\mathbf{qq})\cdot\mathbf{v}$, allowing the two velocity factors to be taken outside the integral, whereas $(\mathbf{qq})$ should be treated as the outer (or dyadic) product inside the integral, viz.,

$$\iint d^2\mathbf{q}\,(\mathbf{q}\cdot\mathbf{v})^2\cdots \equiv \mathbf{v}\cdot\left(\iint d^2\mathbf{q}\,(\mathbf{qq})\cdots\right)\cdot\mathbf{v}. \tag{21}$$

Using the above rearrangement in Eq. (7) yields an expression for $\langle P_{\rm imp}\rangle$ that may be directly equated with the Joule power $P_{\rm J}$ in Eq. (1) and, taking into account the fact the velocity $\mathbf{v} = -\mathbf{v}_d$ is *arbitrary*, one may deduce an expression for the

inverse of the drift mobility tensor as

$$\overleftrightarrow{\mu}^{-1} = \frac{\hbar}{e}\frac{n_{\rm imp}}{n}k_{\rm TF}^2 \iint \frac{d^2\mathbf{q}}{2\pi}\,(\hat{\mathbf{q}}\hat{\mathbf{q}})\mathcal{S}(q)\left[\frac{\epsilon_{\rm bg}(q)e^{-qh}}{\epsilon_{\rm bg}^0\epsilon_{\rm stat}(\mathbf{q})}\right]^2 \times \frac{1}{Q}\frac{H(2k_{\rm F}-Q)}{\sqrt{(2k_{\rm F})^2-Q^2}}, \tag{22}$$

where $(\hat{\mathbf{q}}\hat{\mathbf{q}})$ is the outer product of two unit vectors $\hat{\mathbf{q}} = \mathbf{q}/q$, and Q is a function of the wave vector $\mathbf{q}$ given in Eq. (16). The above formula is the main result of our implementation of the ELM that replaces a typical procedure of the BTE approach, which resorts to numerical solution of an integral equation for the direction-dependent MRT, followed by an integration of such MRT to obtain numerical values of the mobility tensor components for a preassigned set of the model parameters [12,14–16].

The integration in Eq. (22) may be performed in polar coordinates, $\mathbf{q} = \{q\cos\theta, q\sin\theta\}$, wherefrom switching to a double angle, $\phi = 2\theta$, helps show that the inverse mobility tensor is diagonal, with the components $1/\mu_{xx}$ and $1/\mu_{yy}$ being the inverses of the mobilities along the AC and the ZZ directions, respectively. Furthermore, changing the wave number according to $q = 2k_{\rm F}\frac{\sin\gamma}{b(\phi)}$, where

$$b(\phi) = \sqrt{\frac{m_y+m_x}{2m_d} + \frac{m_y-m_x}{2m_d}\cos\phi}, \tag{23}$$

makes it possible to express the inverse mobility components as a double integral over the angles γ and ϕ,

$$\frac{1}{\mu_{xx/yy}} = 4\frac{\hbar}{e}n_{\rm imp}\int_0^{\pi/2}d\gamma\int_0^{\pi}d\phi\,\mathcal{S}^*\left[\frac{\epsilon_{\rm bg}^*}{\epsilon_{\rm bg}^0}e^{-2k_{\rm F}h\frac{\sin\gamma}{b}}\right]^2 \times \frac{(1\pm\cos\phi)\sin^2\gamma}{(b^2+\epsilon_{\rm bg}^* b\nu\sin\gamma + a\nu^2\sin^2\gamma)^2}, \tag{24}$$

where $\nu = 2k_{\rm F}/k_{\rm TF}$, $\mathcal{S}^*$ and $\epsilon_{\rm bg}^*$ stand for functions of γ and ϕ that are obtained by substituting $q = 2k_{\rm F}\frac{\sin\gamma}{b(\phi)}$ in the original functions $\mathcal{S}(q)$ and $\epsilon_{\rm bg}(q)$, and a stands for the auxiliary function

$$a(\phi) = \pi k_{\rm TF}[\alpha_x+\alpha_y+(\alpha_x-\alpha_y)\cos\phi], \tag{25}$$

whereas the $\pm$ sign in Eq. (24) refers to the AC/ZZ direction.

While the integral in Eq. (24) is easily computed numerically for a general set of parameters, it is of interest to take advantage of its analytical tractability and consider its limiting forms for small and large carrier density n, where the dependence on n can be factored out from the dependence on the effective masses of charge carriers. In such limiting cases, the mobility components may be approximately written as $\mu_{xx/yy} = P_{x/y}(n)M_{x/y}^{(\ell)}$, where the latter factor is defined by

$$M_{x/y}^{(\ell)} = \left[\frac{1}{\pi}\int_0^{\pi}d\phi\,\frac{(1\pm\cos\phi)}{b^{\ell}(\phi)}\right]^{-1}, \tag{26}$$

with $b(\phi)$ given in Eq. (23) and ℓ being an integer. When such factorization is possible, the mobility asymmetry ratio becomes independent of n and is given by $\mu_{xx}/\mu_{yy} = M_x^{(\ell)}/M_y^{(\ell)} \equiv \mathcal{R}_\ell$, which happens to be an increasing function of ℓ.

For example, in the limit of zero doping of phosphorene ($n \to 0$, the "complete screening" approximation [16]), we find for planar distribution of impurities that the factor $P_{x/y}(n)$ is independent of n and is given by

$$P_{x/y}^0 = \frac{e}{\pi^2\hbar}\frac{1}{n_{\rm imp}S_{\rm HD}(0)}, \tag{27}$$

while the corresponding effective mass factor is $M_{x/y}^{(4)} = \frac{m_d}{m_{x/y}}$. Thus, the mobility components at zero density are expected to approach $\mu_{xx/yy}^0 \approx P_{x/y}^0 M_{x/y}^{(4)}$ for sufficiently low density and thereby exhibit the anisotropy ratio of $\mathcal{R}_4 = m_y/m_x$. This result is valid when $k_{\rm F}^{-1}$ is the longest length scale in a structure with planar impurity distribution, i.e., when $2k_{\rm F} \ll \min(k_{\rm TF}, \frac{1}{d}, \frac{1}{h}, \frac{1}{2\pi\alpha_x}, \frac{1}{2\pi\alpha_y}, \frac{2\pi}{r_c})$, and it is also valid for a distribution of uncorrelated impurities over finite thickness L when $r_c/(2\pi)$ is replaced by L in this list while setting $S_{\rm HD}(0) = 1$ in Eq. (27).

Interestingly, Eq. (27) shows that, while the mobility components are inversely proportional to the average impurity concentration $n_{\rm imp}$ in the absence of correlation among the impurities, i.e., when $S_{\rm HD}(0) = 1$, the presence of the factor $S_{\rm HD}(0) = (1-p)^3/(1+p)$ with the packing fraction $p = \pi n_{\rm imp} r_c^2/4$ gives rise to a U-shaped dependence of $P_{x/y}^0$ on $n_{\rm imp}$ for any given finite value of the correlation distance r_c. This dependence exhibits a well-defined minimum at the impurity concentration $n_{\rm imp} \approx 0.86/(\pi r_c^2)$, corresponding to the packing fraction of $p \approx 0.215$, so that the minimum value that the mobility components can reach in the regime of complete screening is given in terms of r_c by

$$\mu_{xx/yy}^0\big|_{\rm min} \approx 0.93\, r_c^2\,\frac{e}{\hbar}\,\frac{m_d}{m_{x/y}}. \tag{28}$$

We note that $\mathcal{R}_4 = m_y/m_x$ is the largest anisotropy ratio, which can be attained in the limit of zero-carrier density only. It will be shown in the next section that, when this density increases, the anisotropy ratio decreases, which will be discussed by considering various limiting forms of Eq. (24) in the opposite regime of large densities. Depending on the model configuration, the mobility components will be found to scale as $\mu_{xx/yy} \propto \nu^{4-\ell}M_{x/y}^{(\ell)}$ with ℓ taking values 3, 2, and 1, where $\nu = 2k_{\rm F}/k_{\rm TF} \equiv \sqrt{n/n_{\rm TF}}$ with $n_{\rm TF} = k_{\rm TF}^2/(8\pi)$. This will give the sequence of asymmetry ratios $\mathcal{R}_4 > \mathcal{R}_3 > \mathcal{R}_2 > \mathcal{R}_1$ for various configurations at large carrier densities. It should be kept in mind, however, that the regime of large carrier densities is of somewhat academic interest because then the assumption of a single band occupancy and/or the concept of (constant) anisotropic effective electron or hole masses in phosphorene may become questionable.

III. RESULTS

We shall first demonstrate validity of the formula in Eq. (22), that is Eq. (24), by reproducing results reported in Fig. 3 of Ref. [12] and in Fig. 4 of Ref. [16] using the model parameters from those references. We shall then switch in the remainder of this section to the parameters deduced from the *ab initio* data of Ref. [29] for n-doped phosphorene with the electron density of $n = 10^{13}$ cm^{-2}, giving $m_x \approx 0.133\,m_0$

and $m_y \approx 1.119\, m_0$, where m_0 is the free-electron mass, and $\alpha_x = 0.572$ nm and $\alpha_y = 0.488$ nm for static polarizabilities due to interband transitions. Even though the values of the electron effective masses show some variation with the doping density, they remain approximately unchanged up to about $n = 5 \times 10^{13}$ cm^{-2} [29], so we shall take m_x and m_y as constant over the range of n considered here. We note that the hole effective masses exhibit a larger anisotropy than the electron effective masses, but also show more pronounced variation with the doping density in the considered range [29], so we focus on n doped phosphorene to study the effects of variable doping density and different distributions of impurities assuming fixed values of m_x and m_y. For the substrate, we take $\epsilon_s = 3.9$ representing SiO_2.

In Fig. 1, we used Eq. (24) with the effective masses $m_x = 0.15\, m_0$ and $m_y = m_0$ corresponding to the hole masses used in Ref. [12], while setting $\alpha_x = \alpha_y = 0$ and $h = 0$ for uncorrelated impurities ($r_c = 0$) with the areal density $n_{\rm imp} = 10^{12}$ cm^{-2} that occupy a planar layer at three different depths or a layer of thickness $L = 300$ nm in a SiO_2 substrate. Our results for the mobility components are shown with solid lines, whereas the curves from Fig. 3 of Ref. [12] are reproduced with dashed lines. We see an almost complete agreement between the ELM and BTE methods, except for some small discrepancy (of unknown origin) in the mobilities shown in panels (a) and (b) for a planar layer at finite depths $d = 1$ and 2 nm, which is augmented in the plots of the mobility ratio in panel (c) when the doping density exceeds $\sim 10^{13}$ cm^{-2}.

At the lowest doping density in Figs. 1(a) and 1(b), the mobility curves show a tendency to level off at a constant value implied by Eq. (27) with $S_{\rm HD}(0) = 1$, whereas the asymmetry ratio of $\mu^0_{xx}/\mu^0_{yy} = \mathcal{R}_4 \approx 6.7$ can be reached in Fig. 1(c) for a density below some critical value that depends on the selection of the model parameters [see the conditions of validity for Eq. (27)]. As the density increases, the mobility components also increase in Figs. 1(a) and 1(b), but their ratio tends to decrease in Fig. 1(c). This is a consequence of the increased screening of impurities due to the intraband electron transitions in phosphorene, which apparently tends to reduce the effects of asymmetry in the effective masses in a manner that is modulated by varying the distance between the impurities and phosphorene. In the cases of a planar layer at zero depth and impurities occupying a thick layer in the substrate, the ratio decreases monotonically, but in the case when a planar layer is at finite depth, the ratio exhibits a minimum, which occurs in Fig. 1(c) at a density in a range between $\sim 10^{13}$ and 10^{14} cm^{-2} when $d = 1$ and 2 nm.

In the case of uncorrelated impurities occupying a layer of thickness L, an expression for the mobility can be deduced from Eq. (24) when $k_{\rm F}^{-1}$ is still the longest length scale in the structure, except for the condition $2Lk_{\rm F} \gg 1$. We find then that the mobility components may be approximated by $\mu_{xx/yy} = \frac{e}{2\pi\hbar}\frac{\bar{L}v}{n_{\rm imp}} M^{(3)}_{x/y}$, where $\bar{L} = k_{\rm TF}L$. This exhibits the scaling $\mu_{xx/yy} \propto \sqrt{n}$ and gives an asymmetry ratio of $\mathcal{R}_3 \approx 4.2$ at an intermediate doping density, which seems to apply in the region around $n = 10^{11}$ cm^{-2} in Fig. 1(c). On the other hand, for this model of the impurity distribution, the dependencies on n and the effective masses cannot be factored at large doping densities.

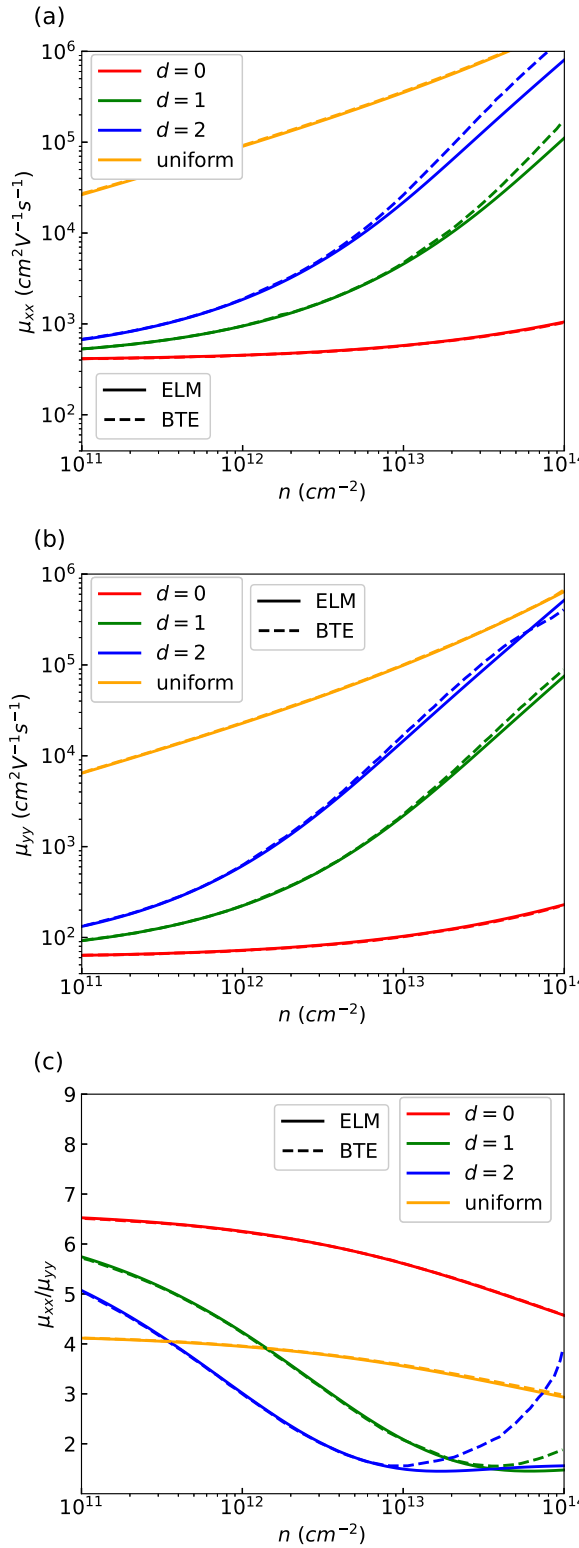

FIG. 1. Mobilities along (a) x-axis, (b) y-axis, and (c) their ratio vs carrier density n using the ELM (solid curves) and the BTE (dashed curves) of Ref. [12] for impurities with the density $n_{\rm imp} = 10^{12}$ cm^{-2} and zero correlation, which occupy a plane at the depth $d = 0$ (red), $d = 1$ nm (green), and $d = 2$ nm (blue) and are uniformly distributed over the layer of thickness $L = 300$ nm (orange) in a SiO_2 substrate with the gap $h = 0$. The parameters are taken from Ref. [12].

In the case of a planar layer of uncorrelated impurities with $d = 0$ in Fig. 1, taking the limit of large doping density, such that $\nu \gg 1$ in Eq. (24), we find $\mu_{xx/yy} = \frac{e}{2\pi^2\hbar}\frac{(\epsilon^0_{\rm bg}\nu)^2}{n_{\rm imp}}M^{(2)}_{x/y}$, where $M^{(2)}_{x/y} = (\sqrt{m_x} + \sqrt{m_y})/(2\sqrt{m_{x/y}})$. This implies the scaling $\mu_{xx/yy} \propto n$ for $n \gg n_{\rm TF}$ and gives the asymmetry ratio of $\mathcal{R}_2 = \sqrt{m_y/m_x} \approx 2.6$ [16], which is smaller than the ratio $\mathcal{R}_4 = m_y/m_x \approx 6.7$ for $n \to 0$, but is only reached slowly at densities far exceeding those shown in Fig. 1(c).

In the case when a planar layer has finite depth, the occurrence of the minima in the asymmetry ratio in Fig. 1(c) for $d = 1$ and 2 nm was attributed in Ref. [12] to the factor e^{-2qd} in the impurity scattering potential of the BTE method, and the densities where the minima occur were estimated to be $n \sim 1/(2\pi d^2)$. However, while the mobility ratio curves from the BTE method in Fig. 1(c) exhibit sharp upturns for densities exceeding those at the minimum points and they reach the values of $\mu_{xx}/\mu_{yy} \approx 1.9$ and 3.6 at $n = 10^{14}$ cm^{-2} for the depths of $d = 1$ and 2 nm, respectively, the minima in the corresponding mobility ratios from the ELM occur at similar densities, but are rather shallow and, instead of a sharp upturn, the ratios quickly settle at a constant value when n exceeds the densities at the minimum points. This is the main discrepancy between the BTE and ELM, which requires further analysis of both approaches. Here, we only comment on the limiting behavior of the mobility components in the ELM, which may be obtained from Eq. (24) with $\mathcal{S}(q) = e^{-2qd}$ in the limit of large carrier densities. Namely, assuming that $2k_{\rm TF}d \gg 1$ and $2k_{\rm F}d \gg 1$, we obtain $\mu_{xx/yy} \approx \frac{e}{\pi\hbar}\frac{\nu^3}{n_{\rm imp}}\bar{d}(\bar{d} + \epsilon^0_{\rm bg})^2 M^{(1)}_{x/y}$, where $\bar{d} = k_{\rm TF}d$. This gives the scaling $\mu_{xx/yy} \propto n^{3/2}$ for $n \ll 1/(8\pi d^2)$ and the asymmetry ratio of $\mathcal{R}_1 \approx 1.6$, which is (almost) reached in Fig. 1(c) at the density 10^{14} cm^{-2} for both $d = 1$ and 2 nm. We note that $\mathcal{R}_1$ may be evaluated from Eq. (26) in an analytic form for an arbitrary set of effective masses, and it represents the lowest attainable value of the asymmetry ratio, which can apparently be reached only for a planar distribution of impurities at *finite* depth for sufficiently large doping density.

We also used Eq. (24) to calculate the resistivity components, defined as $\rho_{xx/yy} = (en\mu_{xx/yy})^{-1}$, by using the electron mass ratios of $m_y/m_x = 10$ and 2 of Ref. [16] for free phosphorene with $h = 0$ and planar distribution of uncorrelated impurities at $d = 0$. Our calculations reproduced the curves reported in Fig. 4 of Ref. [16] (not shown), which we take, together with the comparison with Ref. [12] shown in our Fig. 1, as a demonstration that the ELM is indeed a promising and significantly simpler method for computing the drift mobility in an anisotropic 2D material than the BTE. However, there remains the discrepancy, seen in Fig. 1(c) at large carrier densities, between the BTE and ELM asymmetry ratios for a planar layer of uncorrelated impurities at finite depth. This requires further analysis of both the BTE and ELM to reveal whether this discrepancy originates from methodological differences between them or is a consequence of limitation(s) of their respective domains of validity. While this is certainly a worthy project for future work, it should be kept in mind that this discrepancy likely occurs at quite large carrier densities, where several model assumptions used in this work and in those based on the BTE method [12,16] may not be justified.

In Fig. 2 we revert to using the effective electron masses deduced from Ref. [29], both with $\alpha_x = \alpha_y = 0$ (solid curves) and $\alpha_x = 0.572$ nm and $\alpha_y = 0.488$ nm (dashed curves), considering planar impurity distribution at three depths and the gap $h = 0$, as in Fig. 1. A comparison of solid curves in Figs. 1 and 2 shows the effects of changing the effective masses from $m_x \approx 0.15\,m_0$ and $m_y \approx m_0$ to $m_x \approx 0.133\,m_0$ and $m_y \approx 1.119\,n_0$, which is best exposed in the values approached by the mobility ratios for $d = 0$ at the lowest density of $n = 10^{11}$ cm^{-2} shown in those figures. Namely, those curves approach the values $\mathcal{R}_4 = m_y/m_x \approx 6.7$ in Fig. 1(c) and 8.4 in Fig. 2(c), as implied by the condition $n \ll n_{\rm TF}$ for the validity of Eq. (27) in the regime of "complete screening." The fact that the corresponding values of the mobility ratio for finite depths of $d = 1$ and 2 nm are smaller than those for $d = 0$ at $n = 10^{11}$ cm^{-2} indicates that the corresponding condition $n \ll 1/(8\pi d^2)$ can only be reached in those cases at much smaller doping densities.

More importantly, a comparison between the solid and dashed curves in Fig. 2 shows that the effect of screening due to finite values of $\alpha_{x/y}$ from the interband transitions increases in magnitude with increasing doping density. This effect is quite prominent for $d = 0$, i.e., when impurities lie in the plane of phosphorene (given that $h = 0$), giving rise to a more rapid decrease of the asymmetry ratio in Fig. 2(c) with increasing carrier density, reaching a value of $\mu_{xx}/\mu_{yy} \approx 2.5$ at $n = 10^{14}$ cm^{-2}, in contrast to the value $\mu_{xx}/\mu_{yy} \approx 5.5$ for the case with $\alpha_x = \alpha_y = 0$. In fact, it may be deduced from Eq. (24) in the case with $d = 0$ that, for very large densities such that $2\pi k_{\rm F}\min(\alpha_x, \alpha_y) \gg \epsilon^0_{\rm bg} \sim 1$, the dependence of the mobility on n may be approximated by the factor $\mu_{xx/yy} \propto \frac{e}{\pi\hbar}\frac{\nu^3}{n_{\rm imp}}\bar{a}\epsilon^0_{\rm bg}$, where $\bar{a}$ is the angular average of $a(\phi)$ in Eq. (25), but the effective mass dependent factor takes into account asymmetries of both $a(\phi)$ and $b(\phi)$ in Eq. (23). This gives the scaling $\mu_{xx/yy} \propto n^{3/2}$, like in the case of impurities at finite depth d, accompanied by an asymmetry ratio of $\mu_{xx}/\mu_{yy} \approx 1.8$, which is somewhat larger than $\mathcal{R}_1 \approx 1.7$, but can only be reached at densities far exceeding those shown in Fig. 2.

On the other hand, the relative importance of finite $\alpha_{x/y}$ is suppressed by the increasing depth of impurities. This may be rationalized by referring to Eq. (22), where the form factor $\mathcal{S}(q)$ involves a factor e^{-2dq}, which should be compared with the term involving $\alpha_{x/y}$ in the dielectric function in Eq. (9). One may conclude that, while both the screening by the depth in the substrate and the screening by the interband electron transitions in phosphorene cause a decrease of the mobility asymmetry ratio with increasing doping density, the former screening mechanism will prevail because of the exponential dependence in e^{-2dq} whenever the depth of impurities is such that $d \gtrsim \pi \max(\alpha_x, \alpha_y) \approx 1.8$ nm.

The phosphorene layer has a relatively large thickness, which may be qualitatively taken into account by allowing for a finite gap between the effective plane of the charge density in a phosphorene sheet and the nearby dielectric surface. While often a zero gap is assumed between phosphorene and substrate in modeling the transport of charge carriers [12,16], we explore the effects of finite gap h in Fig. 3 for a doping density of $n = 10^{13}$ cm^{-2} by showing variation in the mobilities with changing h such that $h + d = 1$ nm, i.e., by

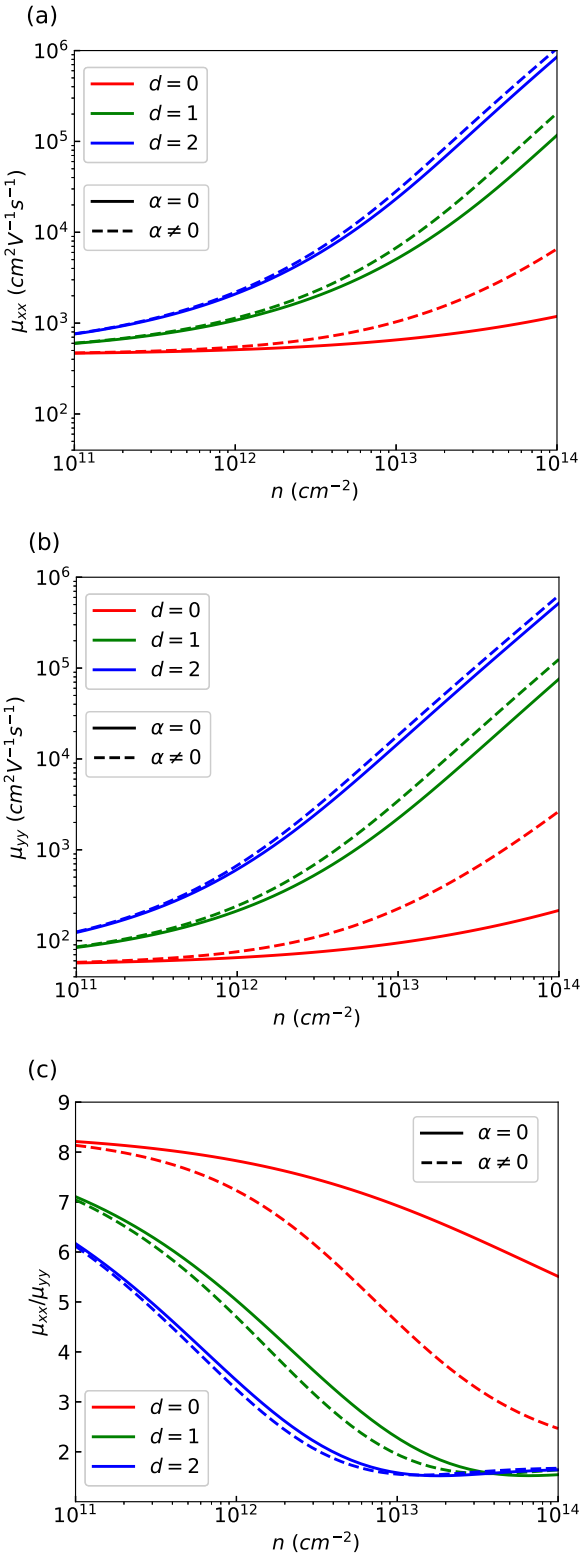

FIG. 2. Mobilities along (a) x-axis, (b) y-axis, and (c) their ratio vs carrier density n using $\alpha_x = \alpha_y = 0$ (solid curves) and nonzero values of polarizabilities α_x and α_y (dashed curves) for impurities with the density $n_{\rm imp} = 10^{12}$ cm^{-2} and zero correlation, which occupy a plane at the depth $d = 0$ (red), $d = 1$ nm (green), and $d = 2$ nm (blue) in a SiO_2 substrate with the gap $h = 0$. The parameters are taken from Ref. [29].

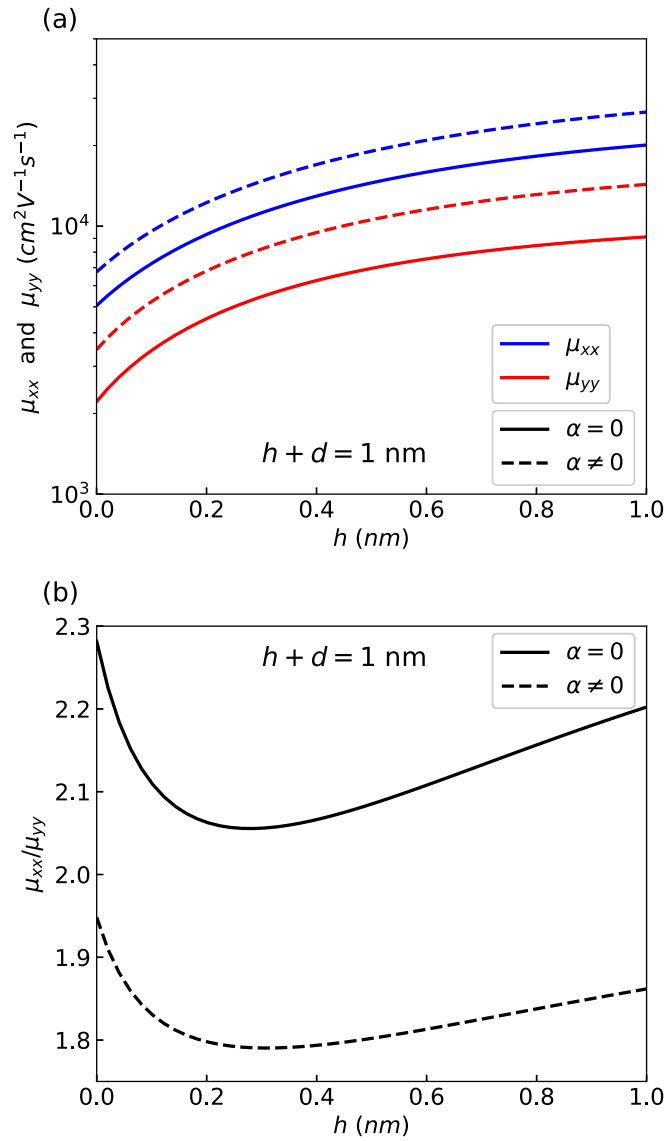

FIG. 3. (a) Mobilities along x-axis (blue) and y-axis (red) and (b) their ratio vs the gap h using $\alpha_x = \alpha_y = 0$ (solid curves) and nonzero values of polarizabilities α_x and α_y (dashed curves) for a fixed doping density of $n = 10^{13}$ cm^{-2} and impurities with the density $n_{\rm imp} = 10^{12}$ cm^{-2} and zero correlation, which occupy a plane at a variable depth d in a SiO_2 substrate, such that the sum $h + d$ is held fixed at 1 nm. The parameters are taken from Ref. [29].

keeping a fixed distance of 1 nm between the charge carriers in phosphorene and uncorrelated impurities with the density $n_{\rm imp} = 10^{12}$ cm^{-2} in a planar layer. While the dependence of the mobility ratio on h in this setting is not strong, it does indicate that the gap size should be included in a more detailed modeling of transport properties in phosphorene. We considered in Fig. 3 the cases of both $\alpha_x = \alpha_y = 0$ (solid curves) and $\alpha_x = 0.572$ nm and $\alpha_y = 0.488$ nm (dashed curves), which seem to mainly provide an offset between the mobility curves, which is comparable in size to their variation with changing h.

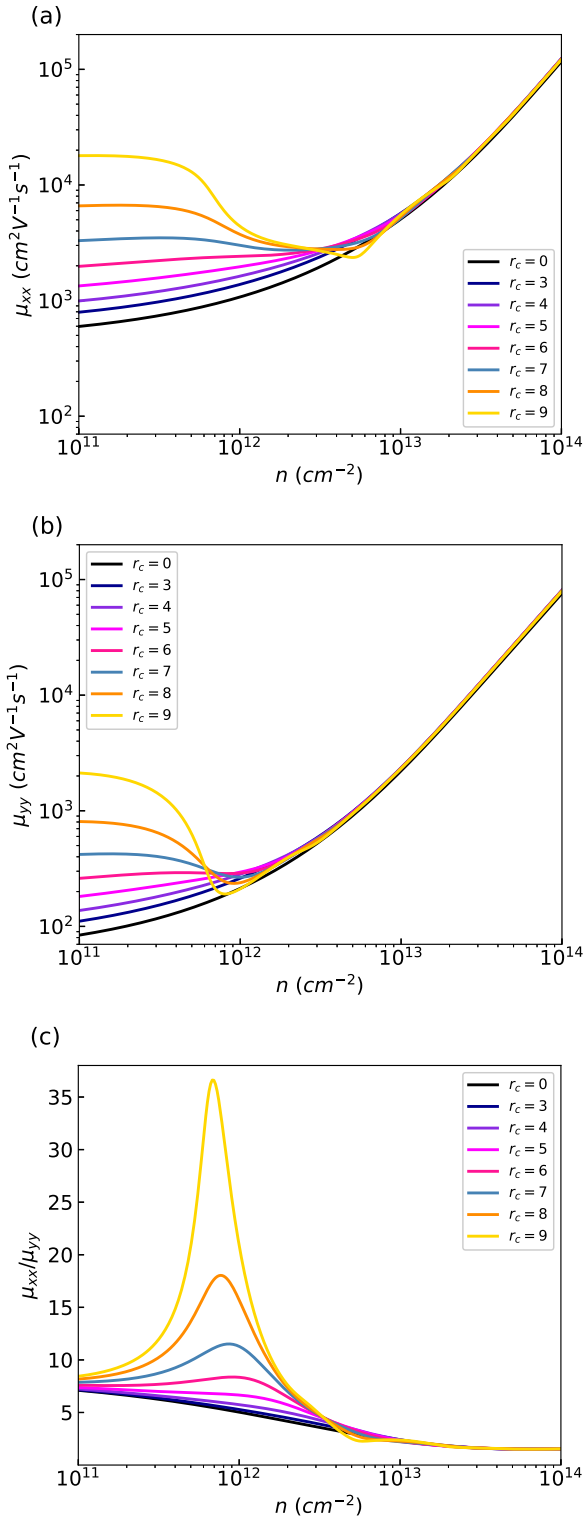

FIG. 4. Mobilities along (a) x-axis, (b) y-axis, and (c) their ratio vs carrier density n using $\alpha_x = \alpha_y = 0$ for impurities with the density $n_{\rm imp} = 10^{12}$ cm^{-2}, which occupy a plane at the depth $d = 1$ nm in a SiO_2 substrate with the gap $h = 0$, for correlation distances $r_c = 0$, 3, 4, 5, 6, 7, 8, and 9 nm. The parameters are taken from Ref. [29].

In Fig. 4, we explore the effects of correlation among the impurities with the density $n_{\rm imp} = 10^{12}$ cm^{-2}, which occupy a plane at the depth $d = 1$ nm for phosphorene where we set $\alpha_x = \alpha_y = 0$, as well as $h = 0$. We chose a range of values for the correlation distance r_c such that the packing fraction stays $p < 0.69$ in this figure. One observes in panels (a) and (b) a large spread of the mobility curves with different r_c values at doping densities n that are roughly smaller than $n_{\rm imp}$, as well as a relatively abrupt congregation of all the curves as the density increases beyond certain critical values that are different for the AC and ZZ directions. This behavior may be understood by noticing the constraint $Q(\mathbf{q}) \equiv qb(\phi) < 2k_{\rm F}$ in Eq. (22) and recalling that the structure factor $\mathcal{S}(q) = S_{\rm HD}(q)e^{-2qd}$ in that equation involves the HD factor $S_{\rm HD}(q)$, which oscillates around the value $S_{\rm HD}(q) = 1$ for small packing fractions p, but is strongly reduced at the wave numbers $q < q_1 = 2\pi/r_c$ for increasing p. Thus, for doping densities, such that $k_{\rm F}r_c \lesssim \pi b(\phi)$, or $n \lesssim \frac{\pi}{2}[b(\phi)/r_c]^2 \equiv n_c(\phi)$, one would expect an increase in the mobility resulting from Eq. (24), which grows in magnitude with increasing r_c, as implied by the long-wavelength limit of $S_{\rm HD}(0) = (1-p)^3/(1+p)$. On the other hand, once the doping density surpasses the critical value n_c, the $\mathbf{q}$-integral in Eq. (22) is increasingly dominated by the regions of large q values, where the HD factor $S_{\rm HD}(q)$ exhibits damped oscillations about the value $S_{\rm HD}(q) = 1$. As a consequence, the effects of finite correlation distance weaken and the mobility curves start to congregate toward the case of uncorrelated impurities as the doping density increases beyond n_c. The role of the peak at q_1 is most prominent at high packing fractions p, as evidenced by the occurrence of the weak local minima in the mobility curves for the correlation distance of $r_c = 9$ nm in Figs. 4(a) and 4(b). The location of those minima may be estimated by setting $\phi = 0$ (AC direction) and $\phi = \pi$ (ZZ direction) in the function $n_c(\phi)$, which yield $n_c^{\rm AC} \approx 5.6 \times 10^{12}$ cm^{-2} and $n_c^{\rm ZZ} \approx 6.7 \times 10^{11}$ cm^{-2}, in close agreement with the local minima observed in the curves with $r_c = 9$ nm in Figs. 4(a) and 4(b), respectively.

In Fig. 4(c), one notices that increasing values of r_c have a relatively weak effect on the mobility ratio, except in a region of the doping densities n near the impurity density $n_{\rm imp}$, where the ratio develops a broad peak with the height that increases with r_c. While this peak is related to different doping densities where the congregation of mobility curves sets in for the AC and ZZ directions, the weak dependence of the mobility ratio on r_c at low doping densities is implied by the formula in Eq. (27) for the regime of "complete screening," where the structure factor $S_{\rm HD}(0)$ is a common factor in both directions. Similarly, the diminishing dependence on r_c at the densities $n \gtrsim 10^{13}$ cm^{-2} in Fig. 4(c) is a consequence of the convergence of the mobility curves to those characterizing uncorrelated impurities, as observed in Figs. 4(a) and 4(b) at $n \gtrsim n_c^{\rm AC}$ and $n \gtrsim n_c^{\rm ZZ}$, respectively.

We have repeated similar calculations with the impurity density increased to $n_{\rm imp} = 10^{13}$ cm^{-2} while choosing a range of the r_c values such that $p < 0.69$. While the overall magnitudes of the mobility components were roughly decreased by a factor of 10, as expected, qualitative behavior of all the curves in such a plot (not shown) remained the same as in Fig. 4, except for all the characteristic features being shifted to increased values of the doping density by a factor of ∼10.

Finally, in Fig. 5, we compare the effects of finite correlation among the impurities with the effects of screening due to the interband electron transitions by juxtaposing the

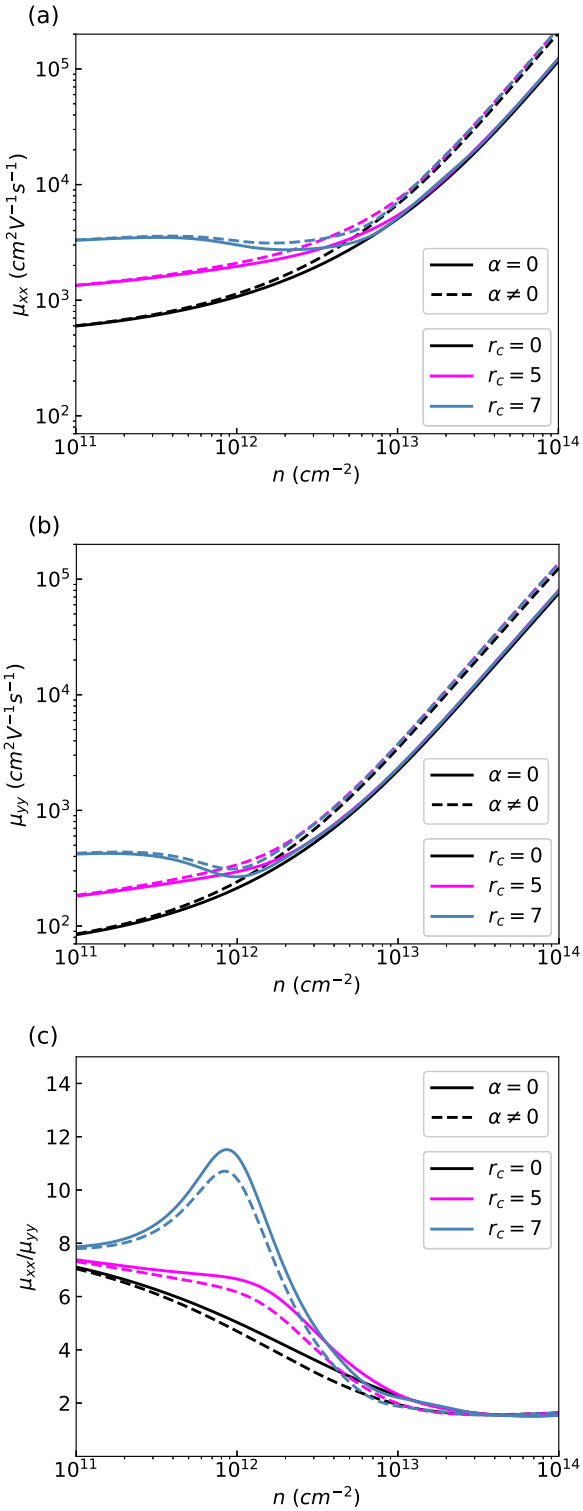

FIG. 5. Mobilities along (a) x-axis, (b) y-axis, and (c) their ratio vs carrier density n using $\alpha_x = \alpha_y = 0$ (solid curves) and nonzero values of polarizabilities α_x and α_y (dashed curves) for impurities with the density $n_{\text{imp}} = 10^{12}$ cm^{-2}, which occupy a plane at the depth $d = 1$ nm in a SiO_2 substrate with the gap $h = 0$, for correlation lengths $r_c = 0$, 5, and 7 nm. The parameters are taken from Ref. [29].

cases of $\alpha_x = \alpha_y = 0$ (solid curves) with $\alpha_x = 0.572$ nm and $\alpha_y = 0.488$ nm (dashed curves) for impurities with the density $n_{\text{imp}} = 10^{12}$ cm^{-2} and a subset of correlation distances r_c taken from Fig. 4. One notices in panels (a) and (b) that the effects of finite $\alpha_{x/y}$ are negligible at small doping densities, where the effects of correlation prevail, while at large doping densities, the curves with different r_c congregate into two distinct groups in a similar manner as in Fig. 4, with the group having finite $\alpha_{x/y}$ values reaching higher values of the mobility than the group having $\alpha_x = \alpha_y = 0$, commensurate with Fig. 2. At the same time, finite values of $\alpha_{x/y}$ cause a relatively small but noticeable reduction of the mobility ratio in the panel (c) in the region of the broad peak that is positioned at a doping density near n_{imp}.

IV. CONCLUDING REMARKS

We have presented an adaptation of the ELM for computation of the drift mobility tensor due to the charged impurity scattering of carriers in an anisotropic 2D material with model parameters pertaining to doped phosphorene on a substrate. By a comparison with the computational data available in the literature that are based on the BTE approach to this problem at zero temperature, we demonstrated that the formula obtained from the ELM is reliable and that it offers a computationally more efficient way for studying the transport properties of such materials. To illustrate the efficiency of the ELM, we explored the effects of random distribution of CIs by means of a structure factor, which naturally arises in the formula for the mobility components obtained in the ELM. In addition, we have amended the density-density polarization function of quasifree charge carriers in doped phosphorene by including a static polarizability tensor with the components α_x and α_y, which arise from the interband electron transitions in phosphorene.

For a planar distribution of impurities, we have found that increasing their depth in the substrate causes an increase of the mobility tensor components and a decrease of their asymmetry ratio as a consequence of weakened interaction with charge carriers. These effects are more pronounced at higher doping densities, indicating an increasing role of static screening due to the intraband electron transitions in phosphorene. This latter mechanism of the impurity screening is augmented by the inclusion of static polarizabilities $\alpha_{x/y}$ due to the interband electron transitions, which is particularly prominent for shallow impurities and increasing doping density. The presence of finite $\alpha_{x/y}$ in phosphorene also causes a reduction of the mobility asymmetry ratio with increasing doping density, similar to the effect of the increasing depth of impurities.

At the same time, the existence of finite correlation distance r_c among the impurities in the hard disk model for a planar layer in the substrate gives rise to an increase in the mobility tensor components with increasing r_c at doping densities below the impurity density, while leaving the mobility asymmetry ratio mainly unchanged in that range of densities. In the limit of zero doping density, known as the complete screening approximation, the dependence of the mobility components on the impurity density exhibits a minimum, which is defined by the value of r_c. On the other hand, at high doping densities that exceed the impurity density, there is a very little effect of the correlation distance in both the mobility components and their asymmetry ratio.

Our work revealed a discrepancy between the BTE and ELM theories in their predictions for the mobility asymmetry ratio at large doping densities for a planar layer of impurities at finite depth in the substrate. While the BTE predicts a minimum followed by a substantial increase of the ratio, we found that the ELM predicts that the mobility ratio should level off at a constant value between 1 and 2 for sufficiently large doping density. While these values are commensurate with those from experimental measurements of the mobility asymmetry in phosphorene [2,9,10], a resolution of the discrepancy in theoretical results warrants further study to better establish the domains of validity for both the BTE and ELM.

Exploring other, more elaborate models of the geometric arrangements of CIs near phosphorene is a natural task for future work. While we have limited our considerations of the geometrical arrangement of the CIs to an isotropic distribution in the directions parallel to phosphorene, it may be interesting to investigate how anisotropic models of the CIs' structure would affect the anisotropy in the mobility tensor of doped phosphorene.

ACKNOWLEDGMENTS

This work was supported by the Natural Sciences and Engineering Research Council of Canada (Grant No. 2023-03397).

APPENDIX A: GREEN'S FUNCTION

We derive the Green's function (GF) of the Poisson equation for a layered structure consisting of two semi-infinite dielectrics with relative dielectric constants ϵ_1 and ϵ_2, which occupy regions $z<0$ and $z>0$, respectively, and phosphorene occupying the plane $z=z_0$. The Fourier transform (FT) of the GF, $\widetilde{G}(\mathbf{q};z,z';\omega)$, satisfies the Dyson-Schwinger equation [46]

$$\widetilde{G}(z,z') = \widetilde{G}^{(0)}(z,z') + \frac{1}{4\pi}\int \widetilde{G}^{(0)}(z,z'')\,\check{\mathcal{V}}(z'')\,\widetilde{G}(z'',z')\,dz'', \tag{A1}$$

where we dropped $\mathbf{q}$ and ω in $\widetilde{G}$ and we dropped q in the GF for the structure *without* phosphorene, $\widetilde{G}^{(0)}(q;z,z')$. The presence of phosphorene is included un Eq. (A1) via the interaction "potential" $\check{\mathcal{V}}(z)\equiv -4\pi e^2\chi\,\delta(z-z_0)$, where $\chi\equiv\chi(\mathbf{q},\omega)$ is its density-density polarization function. Thus, the solution of Eq. (A1) is

$$\widetilde{G}(z,z') = \widetilde{G}^{(0)}(z,z') - \frac{e^2\chi\,\widetilde{G}^{(0)}(z,z_0)\,\widetilde{G}^{(0)}(z_0,z')}{1+e^2\chi\,\widetilde{G}^{(0)}(z_0,z_0)}. \tag{A2}$$

Notice that $\widetilde{G}(z,z')\equiv\widetilde{G}_{jk}(z,z')$ and $\widetilde{G}^{(0)}(z,z')\equiv\widetilde{G}^{(0)}_{jk}(z,z')$ are actually tensors, with the indices j,k labeling the cases when the observation point z is in the region $j=1,2$ and the source point z' is in the region $k=1,2$. The components $\widetilde{G}^{(0)}_{jk}(z,z')$ for the structure without phosphorene were obtained in Ref. [46] as

$$\widetilde{G}^{(0)}_{11}(z,z') = \frac{2\pi}{\epsilon_1 q}\left[e^{-q|z-z'|} + \frac{\epsilon_1-\epsilon_2}{\epsilon_1+\epsilon_2}\,e^{q(z+z')}\right], \tag{A3}$$

$$\widetilde{G}^{(0)}_{21}(z,z') = \widetilde{G}^{(0)}_{12}(z',z) = \frac{4\pi}{(\epsilon_1+\epsilon_2)q}e^{-q(z-z')}, \tag{A4}$$

$$\widetilde{G}^{(0)}_{22}(z,z') = \frac{2\pi}{\epsilon_2 q}\left[e^{-q|z-z'|} + \frac{\epsilon_2-\epsilon_1}{\epsilon_1+\epsilon_2}\,e^{-q(z+z')}\right]. \tag{A5}$$

We only require the $\widetilde{G}_{11}(z,z')$ component of the GF in region 1 with $\epsilon_1=\epsilon_s$ where the impurities reside, while phosphorene is placed at a position $z_0=h>0$ in region 2 where we set $\epsilon_2=1$. Thus, from Eq. (A2) we get $\widetilde{G}_{11}(z,z') = \widetilde{G}^{(0)}_{11}(z,z') + \widetilde{G}_{\rm pol}(z,z')$, where the part of the GF due to polarization of phosphorene may be written as

$$\begin{aligned}\widetilde{G}_{\rm pol}(z,z') &= -\frac{e^2\chi\,\widetilde{G}^{(0)}_{12}(z,h)\,\widetilde{G}^{(0)}_{21}(h,z')}{1+e^2\chi\,\widetilde{G}^{(0)}_{22}(h,h)} \\ &= \frac{2\pi}{q}\left[\frac{1}{\epsilon(\mathbf{q},\omega)}-\frac{1}{\epsilon_{\rm bg}(q)}\right]\left[\frac{\epsilon_{\rm bg}(q)}{\epsilon^0_{\rm bg}}\right]^2 e^{q(z+z'-2h)},\end{aligned} \tag{A6}$$

with $\epsilon(\mathbf{q},\omega)$ given in Eq. (9), and the background dielectric function at the location of phosphorene $\epsilon_{\rm bg}(q)$ given in Eq. (8). Notice that the latter quantity is defined by $\epsilon_{\rm bg}(q) = 2\pi/[q\widetilde{G}^{(0)}_{22}(q;h,h)]$ with the use of $\widetilde{G}^{(0)}_{22}(q;h,h)$ from Eq. (A5). Upon using Eq. (A6) in Eq. (6), we invoke the symmetry properties $\chi(-\mathbf{q},-\omega)=\chi^*(\mathbf{q},\omega)$ and accordingly $\widetilde{G}_{\rm pol}(-\mathbf{q};z,z';-\omega) = \widetilde{G}^*_{\rm pol}(\mathbf{q};z',z;\omega)$, along with $\delta\widetilde{\rho}_0(-\mathbf{q},z) = \delta\widetilde{\rho}^*_0(\mathbf{q},z)$, where $*$ indicates complex conjugate, and recall that $\widetilde{G}^{(0)}_{jk}(q;z,z')$ are real-valued, enabling us to derive Eq. (7) featuring the loss function along with the (real-valued) structure factor in Eq. (10).

APPENDIX B: STRUCTURE FACTOR

Notice that the definition of the effective 2D structure factor in Eq. (10) involves a double integral of the autocovariance of the FT, $\widetilde{\rho}_0(\mathbf{q},z)$, of the random function $\rho_0(\mathbf{r},z)$ in Eq. (11), which can be decomposed as

$$\int dz\int dz'\,e^{q(z+z')}\langle\delta\widetilde{\rho}_0(-\mathbf{q},z)\delta\widetilde{\rho}_0(\mathbf{q},z')\rangle = \int dz\int dz'\,e^{q(z+z')}\langle\widetilde{\rho}_0(-\mathbf{q},z)\widetilde{\rho}_0(\mathbf{q},z')\rangle - \left|\int dz\,e^{qz}\langle\widetilde{\rho}_0(\mathbf{q},z)\rangle\right|^2. \tag{B1}$$

We evaluate the first term in the right-hand side of the above equation involving the autocorrelation of $\widetilde{\rho}_0(\mathbf{q},z)$ by means of a classical N-particle joint probability density for impurity positions, $F_N(\mathbf{r}_1,z_1;\mathbf{r}_2,z_2;\ldots;\mathbf{r}_N,z_N)$, which gives rise to the reduced one- and two-particle distribution functions, defined in Eqs. (12) and (13). After taking the FT of Eq. (11),

we obtain

$$\int dz \int dz'\, e^{q(z+z')}\langle\widetilde{\rho}_0(-\mathbf{q},z)\widetilde{\rho}_0(\mathbf{q},z')\rangle$$

$$= e^2Z^2\int\int\cdots\int d^2\mathbf{r}_1dz_1\,d^2\mathbf{r}_2dz_2\,\cdots d^2\mathbf{r}_Ndz_N\,F_N(\mathbf{r}_1,z_1;\mathbf{r}_2,z_2;\ldots;\mathbf{r}_N,z_N)\left[\sum_{j=1}^{N}e^{2qz_j}+\sum_{j=1}^{N}\sum_{k=1,k\neq j}^{N}e^{i\mathbf{q}\cdot(\mathbf{r}_j-\mathbf{r}_k)}e^{q(z_j+z_k)}\right] \tag{B2}$$

$$= e^2Z^2\left[\iint d^2\mathbf{r}\int dz\,e^{2qz}F_1(\mathbf{r},z)+\iint d^2\mathbf{r}_1\iint d^2\mathbf{r}_2\,e^{i\mathbf{q}\cdot(\mathbf{r}_1-\mathbf{r}_2)}\int dz_1\int dz_2\,e^{q(z_1+z_2)}F_2(\mathbf{r}_1,z_1;\mathbf{r}_2,z_2)\right] \tag{B3}$$

$$= e^2Z^2\left[\frac{N}{A}\iint d^2\mathbf{r}\int dz\,e^{2qz}f_1(z)+\frac{N(N-1)}{A^2}\iint d^2\mathbf{r}_1\iint d^2\mathbf{r}_2\,e^{i\mathbf{q}\cdot(\mathbf{r}_1-\mathbf{r}_2)}\int dz_1e^{qz_1}f_1(z_1)\right.$$

$$\left.\times\int dz_2\,e^{qz_2}f_1(z_2)\,g(\|\mathbf{r}_1-\mathbf{r}_2\|;z_1,z_2)\right] \tag{B4}$$

$$= Ne^2Z^2\big[\mathcal{S}(q)+(2\pi)^2n_{\rm imp}\delta(\mathbf{q})\big], \tag{B5}$$

where $\mathcal{S}(q)$ is expressed in Eq. (14) in terms of the *pair correlation* function, $g(r;z_1,z_2)-1$ [36]. Next, we notice that the average of the function $\rho_0(\mathbf{r},z)$ is given by $\langle\rho_0(\mathbf{r},z)\rangle\equiv\bar{\rho}_0(z)=n_{\rm imp}Zef_1(z)$, so that the second term in Eq. (B1) may be evaluated as

$$\left|\int dz\,e^{qz}\langle\widetilde{\rho}_0(\mathbf{q},z)\rangle\right|^2=\left|\iint d^2\mathbf{r}\,e^{-i\mathbf{q}\cdot\mathbf{r}}\right|^2\left|\int dz\,e^{qz}\bar{\rho}_0(z)\right|^2=(2\pi)^2A\,\delta(\mathbf{q})\left|\int dz\,e^{qz}\bar{\rho}_0(z)\right|^2, \tag{B6}$$

where in the last integral one may set $q=0$ because of the δ function and use $\int dz\,\bar{\rho}_0(z)=n_{\rm imp}Ze$ to obtain an expression that cancels out the second term in Eq. (B5) after both Eqs. (B5) and (B6) are inserted into the right-hand side of Eq. (B1).

[1] L. Li, Y. Yu, G. J. Ye, Q. Ge, X. Ou, H. Wu, D. Feng, X. H. Chen, and Y. Zhang, Nat. Nanotechnol. **9**, 372 (2014).
[2] F. Xia, H. Wang, and Y. Jia, Nat. Commun. **5**, 4458 (2014).
[3] H. Liu, A. T. Neal, Z. Zhu, Z. Luo, X. Xu, D. Tománek, and P. D. Ye, ACS Nano **8**, 4033 (2014).
[4] A. Carvalho, M. Wang, X. Zhu, A. S. Rodin, H. Su, and A. H. Castro Neto, Nat. Rev. Mater. **1**, 16061 (2016).
[5] B. Li, C. Lai, G. Zeng, D. Huang, L. Qin, M. Zhang, M. Cheng, X. Liu, H. Yi, C. Zhou *et al.*, Small **15**, 1804565 (2019).
[6] C. Wang, G. Zhang, S. Huang, Y. Xie, and H. Yan, Adv. Opt. Mater. **8**, 1900996 (2020).
[7] G. Zhang, S. Huang, F. Wang, and H. Yan, Laser Photon. Rev. **15**, 2000399 (2021).
[8] Y. Cao, A. Mishchenko, G. L. Yu, E. Khestanova, A. P. Rooney, E. Prestat, A. V. Kretinin, P. Blake, M. B. Shalom, C. Woods *et al.*, Nano Lett. **15**, 4914 (2015).
[9] A. Mishchenko, Y. Cao, G. Yu, C. R. Woods, R. V. Gorbachev, K. S. Novoselov, A. K. Geim, and L. S. Levitov, Nano Lett. **15**, 6991 (2015).
[10] N. Haratipour, Y. Liu, R. J. Wu, S. Namgung, P. P. Ruden, K. A. Mkhoyan, S.-H. Oh, and S. J. Koester, IEEE Trans. Electron Dev. **65**, 4093 (2018).
[11] G. Gaddemane, W. G. Vandenberghe, M. L. Van de Put, S. Chen, S. Tiwari, E. Chen, and M. V. Fischetti, Phys. Rev. B **98**, 115416 (2018).
[12] Y. Liu, T. Low, and P. P. Ruden, Phys. Rev. B **93**, 165402 (2016).
[13] Y. Liu and P. P. Ruden, Phys. Rev. B **95**, 165446 (2017).
[14] F. W. Han, W. Xu, L. L. Li, C. Zhang, H. M. Dong, and F. M. Peeters, Phys. Rev. B **95**, 115436 (2017).
[15] S. Park, S. Woo, and H. Min, 2D Mater. **6**, 025016 (2019).
[16] S. Ahn and S. Das Sarma, Phys. Rev. B **103**, 165303 (2021).
[17] M. G. Calkin and P. J. Nicholson, Rev. Mod. Phys. **39**, 361 (1967).
[18] E. Gerlach, Physica Status Solidi B **61**, K97 (1974).
[19] D. Chattopadhyay and H. J. Queisser, Rev. Mod. Phys. **53**, 745 (1981).
[20] E. Gerlach and P. Grosse, Scattering of free electrons and dynamical conductivity, in *Festkörperprobleme 17*, edited by J. Treusch, Advances in Solid State Physics (Springer, Berlin, Heidelberg, 1977), Vol. 17, pp. 157–193.
[21] E. Gerlach, J. Phys. C **19**, 4585 (1986).
[22] B. N. J. Persson, Phys. Rev. B **44**, 3277 (1991).
[23] J.-L. Farvacque, Phys. Rev. B **39**, 1682 (1989).
[24] J.-L. Farvacque, Semicond. Sci. Technol. **10**, 914 (1995).
[25] Z. L. Mišković, K. Akbari, S. Segui, J. L. Gervasoni, and N. R. Arista, Phys. Rev. B **105**, 045408 (2022).
[26] P. Cudazzo, I. V. Tokatly, and A. Rubio, Phys. Rev. B **84**, 085406 (2011).
[27] A. S. Rodin, A. Carvalho, and A. H. Castro Neto, Phys. Rev. B **90**, 075429 (2014).
[28] M. N. Gjerding, L. S. R. Cavalcante, A. Chaves, and K. S. Thygesen, J. Phys. Chem. C **124**, 11609 (2020).
[29] D. Novko, K. Lyon, D. J. Mowbray, and V. Despoja, Phys. Rev. B **104**, 115421 (2021).
[30] Z. L. Mišković, M. Moshayedi, M. R. Preciado Rivas, J. Jakovac, I. Radović, and V. Despoja, Radiat. Eff. Def. Solids **178**, 54 (2023).

[31] R. Aničić and Z. L. Mišković, Phys. Rev. B **88**, 205412 (2013).
[32] A. Kaser and E. Gerlach, Z. Phys. B **98**, 207 (1995).
[33] R. Hertling and E. Gerlach, Z. Phys. B **103**, 85 (1997).
[34] A. L. Asatrian, A. L. Vartanian, and A. A. Kirakosian, Phys. stat. sol. (b) **203**, 169 (1997).
[35] Y. Rosenfeld, Phys. Rev. A **42**, 5978 (1990).
[36] J.-P. Hansen and I. R. McDonald, *Theory of Simple Liquids: With Applications to Soft Matter* (Elsevier/AP, Amsterdam, 2013).
[37] F. Stern, Phys. Rev. Lett. **18**, 546 (1967).
[38] S. Ahn and S. Das Sarma, Phys. Rev. B **103**, 045303 (2021).
[39] A. Bret and C. Deutsch, Phys. Rev. E **48**, 2994 (1993).
[40] Y.-N. Wang and T.-C. Ma, Phys. Lett. A **200**, 319 (1995).
[41] P. F. Maldague, Surf. Sci. **73**, 296 (1978).
[42] F. H. da Jornada, L. Xian, A. Rubio, and S. G. Louie, Nat. Commun. **11**, 1013 (2020).
[43] M. Moshayedi, M. R. P. Rivas, and Z. L. Mišković, Phys. Rev. B **105**, 075429 (2022).
[44] G. A. Marks, D. Blankespoor, and Z. L. Miskovic, Materials **16**, 1150 (2023).
[45] Z. L. Mišković and M. Moshayedi, Phys. Rev. Res. **5**, 033133 (2023).
[46] N. Kang, Master's thesis, University of Waterloo, 2015.